Choice of reference, influence of non-additivity and present challenges in thermodynamic perturbation theory for mixtures

Morten Hammer,[1, a)] Ailo Aasen,[2, 1] Åsmund Ervik,[1] and Øivind Wilhelmsen[2, 1]

[1)] *SINTEF Energy Research, NO-7465 Trondheim, Norway*

[2)] *Norwegian University of Science and Technology, Department of Energy and Process Engineering, NO-7491 Trondheim, Norway*

(Dated: 10 March 2020)

This work revisits the fundamentals of thermodynamic perturbation theory for fluid mixtures. The choice of reference and governing assumptions can profoundly influence the accuracy of the perturbation theory. The SAFT-VR Mie equation of state is used as a basis to evaluate three choices of hard-sphere reference fluids: single component, additive mixture, and non-additive mixture. Binary mixtures of Lennard-Jones fluids are investigated, where the ratios of σ (the distance where the potential is zero) and the ratios of ϵ (the well depth) are varied. By comparing with Monte Carlo simulations and results from the literature, we gauge the accuracy of the different theories . A perturbation theory with a single-component reference gives inaccurate predictions when the σ-ratio differs significantly from unity, but is otherwise applicable. Non-additivity becomes relevant in phase-equilibrium calculations for fluids with high ϵ-ratios, or when the mixing rule of σ incorporates non-additivity through an adjustable parameter. This can be handled in three ways: by using a non-additive hard-sphere reference, by incorporating an extra term in the additive hard-sphere reference, or with a single-component reference when the σ-ratio is close to unity. For σ- and ϵ-ratios that differ significantly from unity, the perturbation theories overpredict the phase equilibrium pressures regardless of reference. This is particularly pronounced in vicinity of the critical region for mixtures with high ϵ-ratios. By comparing with Monte Carlo simulations where we compute the terms in the perturbation theory directly, we find that the shortcomings of the perturbation theory stem from an inaccurate representation of the second and third-order perturbation terms, a_2 and a_3. As mixtures with molecules that differ significantly in size and depths of their interaction potentials are often encountered in industrial and natural applications, further development of the perturbation theory based on these results is an important future work.

[a)]Electronic mail: morten.hammer@sintef.no

I. INTRODUCTION

Statistical Associating Fluid Theory (SAFT) is a popular methodology for predicting the thermodynamic properties of fluids. Founded in perturbation theory, SAFT type of equations of state (EoS) have displayed excellent capabilities of predicting accurately the thermodynamic properties of non-polar fluids,[1,2] polar fluids,[3] electrolytes,[4] liquid crystals,[5] heterocyclic compounds[6] and many other systems.

A variety of SAFT-type of EoS have been presented over the years. The early versions of SAFT EoS were based on a reference system of hard-spheres. In more recent variants, the monomer interactions are modelled by more sophisticated interaction potentials such as square-well,[7,8] Lennard-Jones,[9] Yukawa[10] and Sutherland potentials.[7] For further details, we refer to Gubbins[11,12] for a thorough overview of the history and development of perturbation theory. Huang and Radosz[13] presented an important early application of SAFT for the square-well potential. Later the Lennard-Jones potential,[14,15] variable range potentials[7] and group contribution versions of SAFT were developed.[16–18] The most frequently used variants of SAFT at date are PC-SAFT[1] and SAFT-VR Mie,[2] which use square-well and Mie-potentials, respectively, to describe the monomer interactions. Although PC-SAFT gives impressively accurate predictions of thermodynamic properties for single-component fluids, it is often at the expense of over-predicting the critical temperature and pressure.[19,20] The SAFT-VR-Mie EoS appears to have overcome the challenge of reproducing the critical point of single-component fluids, which is evident by the excellent match between SAFT-VR Mie and simulation data displayed in Fig. 7 in Ref. 2. However, whether a consistent representation of the critical point has been achieved remains to be discussed. In particular, we show in the present work that there are still challenges associated with the representation of the critical behavior of mixtures. In the perturbation theory by Barker and Henderson,[21,22] the reduced, residual Helmholtz energy $a^{\mathrm{res}} = A^{\mathrm{res}}/Nk_{\mathrm{B}}T$ is

$$a^{\mathrm{res}} = a^{\mathrm{HS}} + \beta a_1 + \beta^2 a_2 + \beta^3 a_3 + ..., \tag{1}$$

where A^{res} is the total Helmholtz energy, a^{HS} is the reduced, residual Helmholtz energy of the hard-sphere system, N is the number of particles, $\beta = 1/k_{\mathrm{B}}T$, where k_{B} is Boltzmann's constant and T is the temperature. The quantities a_1, a_2 and a_3 are the first-, second- and third-order perturbation terms, respectively. Higher order perturbation terms are usually omitted.[23]

The vast majority of research published on both perturbation theory and SAFT-type of EoS has focused on single-component fluids, although most fluids of practical relevance are mixtures. Leonard, Barker and Henderson laid the foundation for the perturbation theory of mixtures in 1970.[24] In a seminal paper, they derived a perturbation theory for mixtures from three different references, 1) a pure component hard-sphere fluid, 2) an additive hard-sphere mixture and 3) a non-additive hard-sphere mixture. Later, the Weeks-Chandler-Anderson perturbation theory[25,26] was also extended to mixtures.[27]

The definition of an additive hard-sphere mixture is that the diameter of the cross interaction equals the mean of the pure-fluid diameters, i.e. $d_{12} = (d_{11} + d_{22})/2$, where subscripts 1 and 2 refer to the two hard-sphere fluids. Although an additive hard-sphere mixture makes sense from a physical perspective, it is not optimal for the perturbation theory, as it leads to an extra term in the expression for the Helmholtz energy of the fluid. Leonard et al.[24] argued that the extra-term is small, but did not investigate the influence of this contribution on the prediction of thermodynamic properties. Leonard and coworkers were unable to evaluate possible benefits of incorporating a non-additive hard-sphere reference, as no suitable EoS existed at the time. Since then, excellent EoS for non-additive hard-sphere mixtures have been developed and presented in the literature.[28,29] The extra contribution to the Helmholtz energy from non-additivity has found little application in EoS development,[30,31] and its impact has never before been gauged by use of molecular simulations. In this work, we shall discuss when non-additivity becomes important, and how it should be handled in the perturbation theory. It should be noted that non-additivity and a first order Mayer f-function perturbation theory for binary mixtures have been explored using molecular simulations.[32]

Beyond the hard-sphere reference, the perturbation terms that account for attractive contributions are different for mixtures than in a pure-component system. In particular, the radial distribution function of a hard-sphere mixture differs from that of the pure fluid.[33] In spite of this, a common approximation is to replace the radial distribution function of the mixture with that of the pure hard-sphere fluid.[2] In the present work, we shall evaluate the validity of this approximation.

The perturbation terms, a_1–a_3, can be obtained directly by combining Monte Carlo simulations in the canonical ensemble with the theory by Zwanzig.[34] Van Westen and Gross recently used this methodology to evaluate perturbation terms up to fourth order for the Lennard-Jones (LJ) fluid.[23] In this work we will, for the first time, use the methodology

to study the properties of mixtures of LJ-fluids. For certain combinations of force field parameters, we will demonstrate that state-of-the-art perturbation theory for mixtures fails to represent higher order perturbation terms (a_2 and a_3), which leads to phase equilibrium pressures and compositions that deviate significantly from simulation results. This reveals a potential for improvement that is of importance in practical examples found in nature and industry.

Perturbation theory for mixtures will be discussed in detail in Sec. II, where the state-of-the-art equation of state for Mie-fluids, SAFT-VR Mie will be used as starting point. The simulation methodologies employed in the work are described in Sec. III. Results are presented and discussed in Sec. IV with concluding remarks given in Sec. V.

II. THEORY

The perturbation theory for mixtures will be developed for Mie potentials, where the interaction potential between particle i and j (subscript) is:

$$u_{ij}(r)/(\mathcal{C}(\lambda_{r,ij},\lambda_{a,ij})\epsilon_{ij}) = \frac{(\sigma_{ij})^{\lambda_{r,ij}}}{r^{\lambda_{r,ij}}} - \frac{(\sigma_{ij})^{\lambda_{a,ij}}}{r^{\lambda_{a,ij}}}, \tag{2}$$

where ϵ is the well-depth, σ is the finite distance at which the inter-particle potential is zero, λ_a and λ_r are the attractive and repulsive exponents and

$$\mathcal{C}(\lambda_r,\lambda_a) = \left(\frac{\lambda_r}{\lambda_r-\lambda_a}\right)\left(\frac{\lambda_r}{\lambda_a}\right)^{\frac{\lambda_a}{\lambda_r-\lambda_a}}. \tag{3}$$

We have used the same combining rules for λ_{ij} and σ_{ij} as commonly used for classical Mie fluids,[2] while we have used the geometrical combining rule for ϵ_{ij}:

$$\lambda_{k,ij} - 3 = \sqrt{(\lambda_{k,ii}-3)(\lambda_{k,jj}-3)}, \quad k = \mathrm{a},\mathrm{r}\,, \tag{4}$$

$$\sigma_{ij} = (1-l_{ij})\frac{\sigma_{ii}+\sigma_{jj}}{2}\,, \tag{5}$$

$$\epsilon_{ij} = (1-k_{ij})\sqrt{\epsilon_{ii}\epsilon_{jj}}\,, \tag{6}$$

where k_{ij} and l_{ij} are adjustable parameters, which we have set to zero unless explicitly stated. The most accurate representation presently available for such fluids was presented by Lafitte et al. in 2013,[2] the SAFT-VR Mie EoS. This EoS is based on a third-order Barker–Henderson[21,22] perturbation theory. Lafitte and coworkers evaluated their EoS for single-component fluids, and included the extension to mixtures in an appendix. In this work, we shall use SAFT-VR Mie as basis and discuss the extension to mixtures in further detail.

A. The perturbation theory for mixtures and the description of the hard-sphere reference system

When Leonard et al. extended the perturbation theory by Barker–Henderson to mixtures,[21,24] they derived the governing theory both by using a single-component system and mixtures of hard spheres as references. In the following, we shall recap some of their findings, present the descriptions of the hard-sphere reference systems and discuss the implications for the extension of SAFT-VR Mie to mixtures.

The choice of hard-sphere reference systems will give different hard-sphere diameters. The hard-sphere diameter for the ij-interaction will for the single-component system be d_{pure}. For a additive mixture system it will be d_{ij}, while for the non-additive system it will be δ_{ij}. To simplify notation and discussion we also define a model-independent hard-sphere diameter, $\not{d}_{ij}$.

1. The single-component hard-sphere fluid

Leonard et al. showed that when a single-component hard-sphere fluid is used as reference in the perturbation theory for mixtures,[24] the following diameter should be used:

$$\not{d}_{ij} = d_{\text{pure}} = \sum_i \sum_j x_i x_j \delta_{ij}, \tag{7}$$

where subscript pure refers to the single-component reference system, x_i is the mole-fraction of component i and:

$$\delta_{ij} = \int_0^{\sigma_{ij}} \left[1 - \exp\{-\beta u_{ij}(r)\}\right] dr. \tag{8}$$

The quantity δ_{ij} is often referred to as the effective hard-sphere diameter or the Barker–Henderson diameter. The reduced Helmholtz energy then becomes:

$$\begin{aligned} a^{\text{res}} =& a^{\text{HS}}_{\text{pure}} + \\ & 2\pi\rho\beta \sum_i \sum_j x_i x_j \int_{\sigma_{ij}}^{\infty} g_{\text{pure}}(r) u_{ij}(r) r^2 dr + \mathcal{O}(\beta^2) \end{aligned} \tag{9}$$

where g_{pure} is the radial distribution function of a single-component hard-sphere fluid of radius d_{pure} at density ρ. A subtlety in this formulation is that $g_{\text{pure}}(r) = 0$ for $r < d_{\text{pure}}$ such that the effective limit of the integrals in Eq. (9) is $\max(\sigma_{ij}, d_{\text{pure}})$. This allows the first order attractive term of the mixture to be formulated as a function of the pure component contributions:

$$a_1 = \sum_i \sum_j x_i x_j a_{1,\text{pure},ij}, \tag{10}$$

which is convenient, since the necessary theory to compute

$$a_{1,\text{pure},ij} = 2\pi\rho\beta \int_{\sigma_{ij}}^{\infty} g_{\text{pure}}(r) u_{ij}(r) r^2 dr \tag{11}$$

has been provided in earlier works.[2] Higher order perturbation terms should also be computed with the single-component hard-sphere fluid as reference, and we shall give further details on this in Secs. II B 1-II B 3.

With the single-component hard-sphere fluid as reference, we used the hard-sphere EoS by Carnahan and Starling[35] with the diameter defined by Eq. (7). The reduced residual Helmholtz energy of the hard-sphere system is then:

$$a^{\mathrm{HS}}_{\mathrm{pure}} = \frac{3 - 2\eta_{\mathrm{pure}}}{(1 - \eta_{\mathrm{pure}})^2}, \tag{12}$$

where:

$$\eta_{\mathrm{pure}} = \frac{\pi \rho d^3_{\mathrm{pure}}}{6}. \tag{13}$$

We refer to Ref. 2 for further details.

2. The additive hard-sphere mixture

In the case of a mixture reference of additive hard spheres, we have

$$d_{ij} = d_{ij} = 0.5\left(\delta_{ii} + \delta_{jj}\right). \tag{14}$$

Here, Eq. (14) defines the additive hard-sphere mixture. The reduced Helmholtz energy becomes:

$$\begin{aligned} a^{\mathrm{res}} =& a^{\mathrm{HS}}_{\mathrm{mix}} + a^{\mathrm{Ad}} + \\ & 2\pi\rho\beta \sum_i \sum_j x_i x_j \int_{\sigma_{ij}}^{\infty} g^{ij}_{\mathrm{mix}}(r) u_{ij}(r) r^2 dr + \mathcal{O}(\beta^2), \end{aligned} \tag{15}$$

where subscript mix refers to the additive hard-sphere mixture. The above equation looks similar to Eq. (9), but has two subtle differences. The first key difference is that g^{ij}_{mix} is the radial distribution function between component i and j in the mixture, a quantity that depends not only on composition and density, but also on the temperature, since the relative ratio of diameters that determines the nature of the hard-sphere mixture, d_{ii}/d_{jj} depends on temperature according to Eq. (8). Furthermore, there is an additional term that must be accounted for:

$$a^{\mathrm{Ad}} = -2\rho\pi \sum_i \sum_j x_i x_j d^2_{ij} g^{ij}_{\mathrm{mix},c} \left[d_{ij} - \delta_{ij}\right] \tag{16}$$

where $g_{\mathrm{mix},c}$ is the radial distribution function at contact (subscript c). This term equals zero if $d_{ij} = \delta_{ij}$.

With the additive hard-sphere mixture as reference, the EoS by Boublík[33] and Mansoori et al.[36] was used. The reduced Helmholtz energy of their EoS is defined as following

$$a^{\mathrm{HS}}_{\mathrm{mix}} = \frac{1}{\zeta_0}\left[\frac{3\zeta_1\zeta_2}{1-\zeta_3} + \frac{\zeta_2^3}{\zeta_3(1-\zeta_3)^2} + \left(\frac{\zeta_2^3}{\zeta_3^2} - \zeta_0\right)\ln(1-\zeta_3)\right], \tag{17}$$

with ζ_m calculated according to Eq. (18).

$$\zeta_m = \frac{\pi\rho}{6}\left(\sum_i x_i d_{ii}^m\right), \quad m = 0, 1, 2, 3. \tag{18}$$

To compute the pair correlation function at contact in estimating the term a^{Ad}, we used the expressions presented by Boublík, which is consistent with our choice of EoS for the additive hard-sphere fluid mixture[33]

$$g_{0,c}(d_{ij}) = \frac{1}{1-\zeta_3} + \frac{3\zeta_2}{(1-\zeta_3)^2}\mu_{ij} + \frac{2\zeta_2^2}{(1-\zeta_3)^3}\mu_{ij}^2, \tag{19}$$

where:

$$\mu_{ij} = \frac{d_{ii}d_{jj}}{d_{ii}+d_{jj}}. \tag{20}$$

In Sec. IV, we will consider two implementations of the additive hard-sphere mixture reference:

SAFT-VR Mie: Similar to Ref. 2, we use the reduced Helmholtz energy described by Eq. 17, but omit the additional term (Eq. 16).

Additive hard-sphere mixture reference: The implementation is as described above, with the additional term in Eq. 16 accounted for.

3. The non-additive hard-sphere mixture

When a mixture of non-additive hard spheres is used as reference,

$$d_{ij} = \delta_{ij}, \tag{21}$$

for all the *i*-*j* pairs. In general, $\delta_{ij} \neq 0.5(\delta_{ii}+\delta_{jj})$ and this is why the mixture is referred to as non-additive. The reduced Helmholtz energy becomes:

$$\begin{aligned} a^{\mathrm{res}} =& a_{\mathrm{na}}^{\mathrm{HS}} + \\ & 2\pi\rho\beta\sum_i\sum_j x_i x_j \int_{\sigma_{ij}}^{\infty} g_{\mathrm{na}}^{ij}(r) u_{ij}(r) r^2 dr + \mathcal{O}(\beta^2), \end{aligned} \tag{22}$$

where g_{na} is the radial distribution function of the non-additive mixture.

To develop accurate EoS for non-additive hard-sphere mixtures is an active field of research,[28] and there are several models available.[28,29,37,38] In this work we have chosen the

model by Santos et al.[28] The model is designed to give the correct second and third virial coefficients. The non-additive mixture hard-sphere diameter is given as

$$d_{\mathrm{na}} = \sqrt[3]{\sum_i x_i \delta_{ii}^3}. \tag{23}$$

The packing fraction used in the model is defined as

$$\eta_{\mathrm{na}} = \frac{\pi \rho d_{\mathrm{na}}^3}{6}. \tag{24}$$

The residual compressibility factor is defined as

$$\begin{aligned} Z_{\mathrm{na}}^{\mathrm{res}} =& \frac{\eta_{\mathrm{na}}}{1-\eta_{\mathrm{na}}} \frac{10 d_{\mathrm{na}}^3 \overline{B_2} - 4\overline{B_3}}{6 d_{\mathrm{na}}^6} \\ &+ Z_{\mathrm{pure}}^{\mathrm{res}}\left(\eta_{\mathrm{na}}\right) \frac{\overline{B_3} - d_{\mathrm{na}}^3 \overline{B_2}}{6 d_{\mathrm{na}}^6}. \end{aligned} \tag{25}$$

Here

$$\overline{B_2} = 4 \sum_i \sum_j x_i x_j \delta_{ij}^3, \tag{26}$$

$$\overline{B_3} = \sum_i \sum_j \sum_k x_i x_j x_k \overline{B}_{i,j,k}^3. \tag{27}$$

For $\overline{B}_{i,j,k}$ we have

$$\overline{B}_{i,j,k} = \frac{4}{3}\left(c_{k;ij}\delta_{ij}^3 + c_{j;ik}\delta_{ik}^3 + c_{i;jk}\delta_{jk}^3\right), \tag{28}$$

$$c_{k;ij} = \delta_{k;ij}^3 + \frac{3}{2}\frac{\delta_{k;ij}^2}{\delta_{ij}}\delta_{i;jk}\delta_{j;ik}, \tag{29}$$

$$\delta_{k;ij} = \max\left(\delta_{ik} + \delta_{jk} - \delta_{ij}, 0\right). \tag{30}$$

Defining the volume independent variables

$$A_1\left(T, \boldsymbol{x}\right) = \frac{10 d_{\mathrm{na}}^3 \overline{B_2} - 4\overline{B_3}}{6 d_{\mathrm{na}}^6}, \tag{31}$$

$$A_2\left(T, \boldsymbol{x}\right) = \frac{\overline{B_3} - d_{\mathrm{na}}^3 \overline{B_2}}{6 d_{\mathrm{na}}^6}, \tag{32}$$

the residual compressibility becomes

$$Z_{\mathrm{na}}^{\mathrm{res}} = \frac{\eta_{\mathrm{na}}}{1-\eta_{\mathrm{na}}} A_1\left(T, \boldsymbol{x}\right) + Z_{\mathrm{pure}}^{\mathrm{res}}\left(\eta_{\mathrm{na}}\right) A_2\left(T, \boldsymbol{x}\right). \tag{33}$$

Here we use the Carnahan–Starling EoS[35] to model the residual compressibility factor of the pure fluid, $Z^{\mathrm{res}}_{\mathrm{pure}}(\eta)$. The residual reduced Helmholtz energy per molecule for the non-additive mixture model is found by integrating Eq. (33)

$$\begin{aligned} a^{\mathrm{HS}}_{\mathrm{na}} &= \int_0^{\eta_{\mathrm{na}}} \frac{Z^{\mathrm{res}}_{\mathrm{na}}}{\eta_{\mathrm{na}}} d\eta_{\mathrm{na}} \\ &= -\ln\left(1-\eta_{\mathrm{na}}\right) A_1\left(T,\boldsymbol{x}\right) + a^{\mathrm{HS}}_{\mathrm{pure}}\left(\eta_{\mathrm{na}}\right) A_2\left(T,\boldsymbol{x}\right), \end{aligned} \tag{34}$$

where η_{na} is calculated according to Eq. (24), and $a^{\mathrm{HS}}_{\mathrm{pure}}$ is given by Eq. (12).

B. The perturbation terms

In the following, the expressions for the perturbation terms will be given, which are very similar to those used in SAFT-VR Mie.[2] While the representation of a_1 reproduces results from Monte Carlo simulations for single-component Mie-fluids, appreciable deviations can be observed for a_2 and a_3, as the shown in Figs. 1 and 2 in Ref. 2.

1. The first order perturbation term

The first order perturbation term is calculated by using

$$a_1 = \sum_i \sum_j x_i x_j a_{1,ij}, \tag{35}$$

where $a_{1,ij}$ is described as

$$a_{1,ij} = 2\pi\rho \int_{\sigma_{ij}}^{\infty} g^{\mathrm{HS}}_{d_{ij}}\left(r\right) u_{ij}\left(r\right) r^2 dr. \tag{36}$$

We use an effective packing fraction, which is computed consistently for the three references:

$$\zeta_x = \begin{cases} \eta_{\mathrm{pure}}, & \text{single-component ref.} \\ \zeta_3, & \text{additive mixture ref.} \\ \eta_{\mathrm{na}}, & \text{non-additive mixture ref.} \end{cases} \tag{37}$$

The hard-sphere diameter, d_{ij}, is defined as,

$$d_{ij} = \begin{cases} d_{\mathrm{pure}}, & \text{single-component ref.} \\ d_{ij}, & \text{additive mixture ref.} \\ \delta_{ij}, & \text{non-additive mixture ref.} \end{cases} \tag{38}$$

For the radial distribution function of the hard sphere reference, $g^{\mathrm{HS}}_{\mathit{d}_{ij}}$, we have assumed that the functional form can be approximated by that of the pure fluid. This assumption will be further evaluated in Sec. IV. $g^{\mathrm{HS}}_{\mathit{d}_{ij}}$ is then defined from the pure fluid radial distribution function at the packing fraction given by Eq. (37),

$$g^{\mathrm{HS}}_{\mathit{d}_{ij}} = g^{\mathrm{pure}}\left(\frac{r}{\mathit{d}_{ij}}; \zeta_x\right). \tag{39}$$

The $a_{1,ij}$ is computed as for pure fluids but with different values of the hard-sphere diameter, d_{ij}, depending on the reference. It was shown in Ref. 39, that each Sutherland potential could be correlated using the quantities a_1^{S} and B defined in the following. The only difference from Ref. 39 is in the treatment of a_1^{S} and B, where the integrals are evaluated as both a function of η and ζ_x for mixtures. Dividing through with η_{ij} gives functions of ζ_x only. For mixtures, $\tilde{a}^{\mathrm{S}}_{1,ij}$, takes the form,

$$\begin{aligned}\tilde{a}^{\mathrm{S}}_{1,ij} &= \frac{a^{\mathrm{S}}_{1,ij}\left(\eta_{ij}, \zeta_x; \lambda_{ij}\right)}{\eta_{ij}} \\ &= -12\epsilon_{ij}\left(\frac{1}{\lambda_{ij}-3}\right)\frac{1-\eta_{\mathrm{eff}}\left(\zeta_x;\lambda_{ij}\right)/2}{\left(1-\eta_{\mathrm{eff}}\left(\zeta_x;\lambda_{ij}\right)\right)^3}.\end{aligned} \tag{40}$$

Here, the pair specific effective packing fraction, η_{ij}, is defined as

$$\eta_{ij} = \frac{\pi\rho\mathit{d}_{ij}^3}{6}. \tag{41}$$

$\tilde{B}_{ij}$ takes the following form:

$$\begin{aligned}\tilde{B}_{ij} &= \frac{B_{ij}\left(\eta_{ij}, \zeta_x, x_{0,ij}; \lambda_{ij}\right)}{\eta_{ij}} \\ &= 12\epsilon_{ij}\left(\frac{1-\zeta_x/2}{\left(1-\zeta_x\right)^3}I_{\lambda_{ij}}\left(x_{0,ij}\right) - \frac{9\zeta_x\left(1+\zeta_x\right)}{2\left(1-\zeta_x\right)^3}J_{\lambda_{ij}}\left(x_{0,ij}\right)\right).\end{aligned} \tag{42}$$

The ratio between the pairwise sigma and the hard sphere diameter is defined as the variable, x_0,

$$x_{0,ij} = \frac{\sigma_{ij}}{\mathit{d}_{ij}}. \tag{43}$$

The overall ij pair contribution to a_1 becomes

$$a_{1,ij} = a_{1,\lambda_{a,ij}} - a_{1,\lambda_{r,ij}} \tag{44}$$

where

$$\begin{aligned}a_{1,\lambda_{k,ij}} =& \mathcal{C}\left(\lambda_{a,ij}, \lambda_{r,ij}\right)\eta_{ij}x_{0,ij}^{\lambda_{k,ij}}\cdot \\ &\left[\tilde{a}^{\mathrm{S}}_{1,ij}\left(\zeta_x;\lambda_{k,ij}\right) + \tilde{B}_{ij}\left(\zeta_x, x_{0,ij};\lambda_{k,ij}\right)\right].\end{aligned} \tag{45}$$

2. The second-order perturbation term

The second-order perturbation term has been represented by the same expressions as SAFT-VR Mie,[2] and is calculated from:

$$a_2 = \sum_i \sum_j x_i x_j a_{2,ij}, \tag{46}$$

where $a_{2,ij}$ is described as

$$a_{2,ij} = \pi \rho K^{\mathrm{HS}} (1 + \chi_{ij}) \int_{\sigma_{ij}}^{\infty} g_{d_{ij}}^{\mathrm{HS}}(r) \left(u_{ij}(r)\right)^2 r^2 dr. \tag{47}$$

The integral part is treated in the same manner as $a_{1,ij}$, where the Sutherland integrals are described as functions of η, ζ_x and x_0. The same reduced isothermal compressibility of the hard-sphere EoS, is used for all pair contributions, simply by substituting the pure fluid η with the mixture packing fraction, ζ_x,

$$K^{\mathrm{HS}} = \frac{(1-\zeta_x)^4}{1 + 4\zeta_x + 4\zeta_x^2 - 4\zeta_x^3 + \zeta_x^4}. \tag{48}$$

For the correction factor, $1 + \chi_{ij}$, we introduce an effective packing fraction based on σ, which is computed consistently for the three references

$$\bar{\zeta}_x = \frac{\pi \rho}{6} \sum_i \sum_j x_i x_j \sigma_{ij}^3. \tag{49}$$

The χ_{ij} correlation is calculated as

$$\chi_{ij} = f_1(\alpha_{ij})\, \bar{\zeta}_x + f_2(\alpha_{ij}) \left(\bar{\zeta}_x\right)^5 + f_3(\alpha_{ij}) \left(\bar{\zeta}_x\right)^8. \tag{50}$$

Finally, we define the dimensionless van der Waals energy of the ij interaction as

$$\alpha_{ij} = -\frac{1}{\epsilon_{ij}\sigma_{ij}^3} \int_{\sigma_{ij}}^{\infty} u_{ij}(r)\, r^2\, \mathrm{d}r\,. \tag{51}$$

3. The third-order perturbation term

The third-order perturbation term has been represented by the same expressions as SAFT-VR Mie,[2] and is calculated by using a van der Waals mixing rule

$$a_3 = \sum_i \sum_j x_i x_j a_{3,ij}, \tag{52}$$

where the pair contribution is given as

$$a_{3,ij} = -\epsilon_{ij}^3 f_4\left(\alpha_{ij}\right) \bar{\zeta}_x \exp\left(f_5\left(\alpha_{ij}\right) \bar{\zeta}_x + f_6\left(\alpha_{ij}\right) \bar{\zeta}_x^2\right). \tag{53}$$

Note that for Lennard-Jones fluids, f_1 to f_6 used in Eq. (50) and Eq. (53) are constant parameters. $a_{3,ij}$ is therefore a function of ϵ_{ij} and $\bar{\zeta}_x$, while χ_{ij} is only a function of $\bar{\zeta}_x$.

C. The virial coefficients of mixtures

The virial expansion is defined as:

$$\frac{\beta P}{\rho} = 1 + B\rho + \mathcal{O}(\rho^2), \tag{54}$$

where B is the second virial coefficient. For a mixture, the expression for the second virial coefficient is:[40]

$$B = \sum_i \sum_j x_i x_j B_{ij}, \tag{55}$$

where the pairwise contributions can be obtained from the potential as[40]

$$B_{ij}^{\text{pot}} = -2\pi \int_0^\infty \left(\exp(-\beta u_{ij}(r)) - 1\right) r^2 dr. \tag{56}$$

The mixture second virial coefficient can be obtained from an EoS by use of the relation

$$B^{\text{EoS}} = \lim_{\rho \to 0} \left(\frac{\partial a^{\text{res}}}{\partial \rho}\right)_T. \tag{57}$$

In Sec. IV, we shall discuss in detail the cross-virial coefficient obtained from the different hard-sphere references. The contribution to the second virial coefficient from the hard-sphere reference is especially important as $\beta \to 0$, i.e. at high temperatures where the dispersion terms vanish. In the following we derive the expressions for the different virial coefficients.

Integrating Eq. (56) for a hard-sphere fluid of diameter δ_{ij}, the hard-sphere second virial coefficient becomes:

$$B_{ij}^{\text{HS,pot}} = \frac{2\pi\delta_{ij}^3}{3}. \tag{58}$$

Differentiating Eq. (12) with respect to ρ in the limit $\rho \to 0$ (Eq. (57)), we obtain the mixture virial coefficient for the single-component reference

$$B_{\text{mix}}^{\text{HS}} = \frac{2\pi}{3} d_{\text{pure}}^3. \tag{59}$$

Differentiating Eq. (17) with respect to ρ in the limit $\rho \to 0$, we get the mixture virial coefficient for the additive mixture reference

$$B_{\text{mix}}^{\text{HS}} = \frac{\pi}{6} \sum_{k=1}^{\text{N}} x_k \delta_{kk}^3 + \frac{\pi}{2} \left(\sum_{k=1}^{\text{N}} x_k \delta_{kk} \right) \left(\sum_{k=1}^{\text{N}} x_k \delta_{kk}^2 \right). \tag{60}$$

Differentiating Eq. (34) with respect to ρ in the limit $\rho \to 0$ gives the mixture virial coefficient for the non-additive mixture reference

$$B_{\text{na}}^{\text{HS}} = \frac{\pi}{6} \overline{B_2} = \frac{2\pi}{3} \sum_k \sum_l x_k x_l \delta_{kl}^3. \tag{61}$$

The cross virial-coefficients from the different references can be identified as

$$B_{ij}^{\text{HS}} = \begin{cases} \dfrac{\pi}{3} \dfrac{\left(d_{\text{pure}}^3 - x_i^2 \delta_{ii}^3 - x_j^2 \delta_{jj}^3 \right)}{x_i x_j}, & \text{single-comp. ref.} \\ \dfrac{2\pi}{3} \left(\dfrac{1}{2} \left(\delta_{ii} + \delta_{jj} \right) \right)^3, & \text{add. mix. ref.} \\ \dfrac{2\pi \delta_{ij}^3}{3}, & \text{non-add. mix. ref.} \end{cases} \tag{62}$$

A comparison to Eq. (58) shows that only the non-additive mixture reference gives the correct cross virial-coefficient. All references give the correct pure fluid virial coefficients.

Using the additive hard-sphere mixture as reference, the extra term, a^{Ad} also gives a contribution to the second virial coefficient

$$B_{ij}^{\text{Ad}} = 2\pi d_{ij}^2 \left(\delta_{ij} - d_{ij} \right), \tag{63}$$

which is the first-order correction to B_{ij}^{HS} for the additive reference (Eq. (62)) in the quantity $(\delta_{ij} - d_{ij})$.

III. METHODS

The perturbation theory presented in Sec. II was implemented in the thermodynamic framework described in Ref. 19, where state-of-the-art phase equilibrium calculations enable precise and robust mapping of phase envelopes by use of the algorithms discussed in Refs. 41 and 42. We will next describe the simulation methodologies used for a binary system with Type 1 and 2 molecules. For all simulations, the inter-molecular interactions were truncated at $r_{\text{c}} = 4 \cdot \max(\sigma_1, \sigma_2)$, and standard long-range corrections assuming $g_{\text{mix}}^{ij} = 1$ when $r > r_{\text{c}}$ were applied. Long-range corrections for pure fluid simulations are described in the appendix of Ref. 39, and have been extended and applied to binary mixtures.

A. Monte Carlo simulations of perturbation terms

The perturbation terms of a binary system can be computed directly by canonical Monte Carlo (MC) simulations of a soft-sphere (SS) reference fluid, defined by the positive part of the potential: $u_{ij}^{\mathrm{SS}}(r) = \max(u_{ij}(r), 0)$. By fixing the number of molecules ($N = N_1 + N_2$), temperature and volume, the soft-sphere mixture can be studied using canonical MC simulations, and the negative energy of the Lennard-Jones fluids can be sampled using the soft sphere system configuration to obtain the perturbation terms of the mixture, in accordance with the theory by Zwanzig.[34]

The overall attractive configurational energy of the system, W, is found by summing all the ij-pair interaction energies for particles separated by at least σ_{ij}. The first order (mean attractive energy), second order (energy fluctuations) and third-order perturbation terms are calculated from the formulas given by Zwanzig:[34]

$$a_1 = \frac{\beta}{N}\langle W\rangle_0, \tag{64}$$

$$a_2 = -\frac{\beta^2}{2!N}\Big\langle \left(W - \langle W\rangle_0\right)^2 \Big\rangle_0, \tag{65}$$

$$a_3 = \frac{\beta^3}{3!N}\Big\langle \left(W - \langle W\rangle_0\right)^3 \Big\rangle_0. \tag{66}$$

Here, $\langle\cdot\rangle_0$ denotes the statistical average in the canonical ensemble of a fluid characterized by the soft-sphere reference. The system energy can further be split into contributions from the 11, 22 and 12 interactions

$$\langle W\rangle_0 = \langle W_{11}\rangle_0 + \langle W_{12}\rangle_0 + \langle W_{22}\rangle_0. \tag{67}$$

This enables an assessment of how the different pair interaction potentials contribute to the total energy.

Following van Westen and Gross,[23] who simulated perturbation terms up to fourth order for a pure Lennard-Jones fluid, a cubic box with periodic boundary conditions and $N = 500$ was used for all simulations. To span the compositional space, simulations were run using $N_2 \in \{150, 250, 350\}$, corresponding to mole fractions of Type 2 molecules of 30, 50, 70 %.

Due to the potentially large difference in the diameters of the molecules of Type 1 and 2, the maximum displacements of the two particle types were tuned independently for each species to yield an acceptance ratio in the interval 30 % to 50 %.

One MC cycle consists of one trial move per particle. To equilibrate the system, $2.0 \cdot 10^6$ MC cycles were run. The production phase consisted of 25 blocks each containing $300 \cdot 10^3$ MC cycles. Sampling of the configurational attractive energy was performed every 250 MC move, as a computationally efficient way of improving the accuracy compared to conventionally sampling only when concluding a MC cycle. The mean values and the standard deviations of the sample means were calculated from the production blocks.

B. Gibbs Ensemble Monte Carlo simulations

We performed Gibbs Ensemble Monte Carlo (GEMC) simulations[43–45] of binary mixtures of Lennard-Jones fluids to determine two-phase coexistence densities and compositions. A total of N_{tot} particles, in the range 2000–10000, were distributed across two simulation boxes, and subjected to in-box displacement moves and box-swap moves. The pressure was maintained by adjusting each box volume independently.[43] The maximum volume step size, and the maximum displacement step size for each species and each box were tuned to yield an acceptance ratio between 30% and 50%.

An MC cycle was defined as N_{tot} attempted displacement moves, 2 attempted single-box volume moves, and N_{swap} attempted swap moves. The number N_{swap} was initialized to N_{tot}, and potentially increased so that at least 0.1% of the N_{tot} particles were on average exchanged in a cycle. Following 3×10^4 equilibration cycles, sampling was performed after each 100th MC move during 3×10^5 production cycles.

C. NPT Monte Carlo simulations

The NPT simulations were run with a total of 1000 particles. A cycle was defined as 1000 displacement moves and one volume move, where the maximum step sizes were tuned during equilibration to yield acceptance ratios between 30% and 50%. Following 5×10^4 equilibration cycles, we performed sampling after each 100th MC move during a production run of 5×10^5 cycles.

IV. RESULTS AND DISCUSSION

We consider mixtures of two components interacting via LJ-potentials, referred to as molecules of Type 1 and 2. The i-j interactions are represented by different well-depths, ϵ_{ij}, and positions where the potentials are zero, σ_{ij}. The LJ-potential was chosen because it is among the most frequently used examples in the literature.[2,21] Moreover, accurate representation of the single-component LJ-fluid has been heavily weighted in the development of state-of-the-art perturbation theories due to the abundance of simulation data.[2] The findings of the present work are also relevant for other interaction potentials, such as Mie potentials,[2] or quantum fluids described by Feynman–Hibbs-corrected Mie-potentials.[39,46]

We shall discuss three choices of reference: 1) Single-component, 2) additive mixture and 3) non-additive mixtures of hard-spheres. We shall consider two variants of the additive mixture implementation, one where Eq. 16 has been included, and another where Eq. 16 has been omitted, referred to as SAFT-VR Mie. Special attention will be given to the influence of the choice of hard-sphere reference on the second virial coefficient (Sec. IV A), handling of non-additivity in the mixture interaction potential (Sec. IV B) and challenges in the representation of mixtures with ϵ-ratios (Sec. IV C) and σ-ratios (Sec. IV D) that differ significantly from unity.

If nothing else is stated, we have used the following definitions for the reduced variables:

$$T^* = \frac{k_\mathrm{B}T}{\epsilon_{11}}, \tag{68}$$

$$P^* = \frac{P\sigma_{11}^3}{\epsilon_{11}}, \tag{69}$$

$$\rho^* = \frac{N_1^2\sigma_{11}^3 + 2N_1N_2\sigma_{12}^3 + N_2^2\sigma_{22}^3}{NV}, \tag{70}$$

where N_1 and N_2 are the number of particles of species 1 and 2, respectively, $N = N_1 + N_2$, and V is the volume of the simulation box.

A. The hard-sphere contribution to the second virial coefficient

Equation (56) shows the connection between the second virial coefficient and the underlying interaction potential. Hence, a comparison of the perturbation theory to Eq. (56) gauges how well the underlying potential is represented. The hard-sphere contribution to

the cross-virial coefficient can be computed exactly, and is given by Eq. (58). The contribution to the second virial coefficient from the hard-sphere reference is especially important at high temperatures where the dispersion terms vanish.

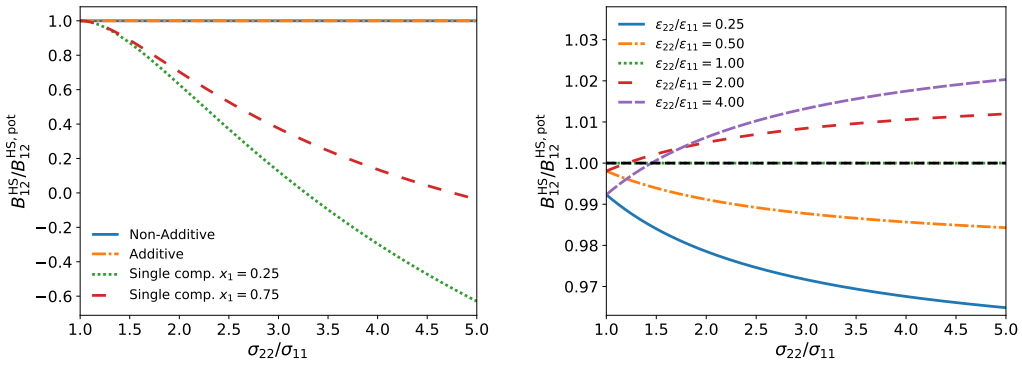

(a) $\epsilon_{22}/\epsilon_{11} = 1.0$ (b) Additive mixture reference

FIG. 1. The hard-sphere contribution to the cross second virial coefficient of the mixture from different hard-sphere reference systems, B_{12}^{HS}, relative to the exact value, $B_{12}^{\mathrm{HS,pot}}$. The plots are made at $T^* = Tk_{\mathrm{B}}/\epsilon_{12} = 1.0$ for different LJ-fluids. Fig. 1a displays all of the hard-sphere reference models. The single-component reference is plotted at two different mole fractions, i.e. $x_1 = 0.25$ and $x_1 = 0.75$, to illustrate the compositional dependence. Fig. 1b shows only the additive mixture reference, plotted for different $\epsilon_{22}/\epsilon_{11}$ ratios.

In Sec. II C, we showed that the hard-sphere cross-virial coefficients from the different references were given by the analytical expressions in Eq. (62). While the non-additive reference reproduces the exact result given by Eq. (58), the other references give different expressions. Fig. 1 compares the hard-sphere contribution to the cross second virial coefficient from different references for different LJ fluids at $T^* = 1$. Fig. 1a shows that the deviation between the single-component reference and the exact result becomes larger with increasing difference in size between the particles of the fluids, i.e. an increasing σ_{22}/σ_{11} ratio. Already at $\sigma_{22}/\sigma_{11} = 1.5$, the error in the representation of the hard-sphere contribution to the cross virial coefficient exceeds 10%. Fig. 1a shows that the choice of reference places a constraint on how accurately thermodynamic properties can be represented by the perturbation theory. The single-component reference should clearly be avoided when describing mixtures with molecules that differ much in size.

A zoom-in on the results from the additive hard-sphere reference displayed in Fig. 1b,

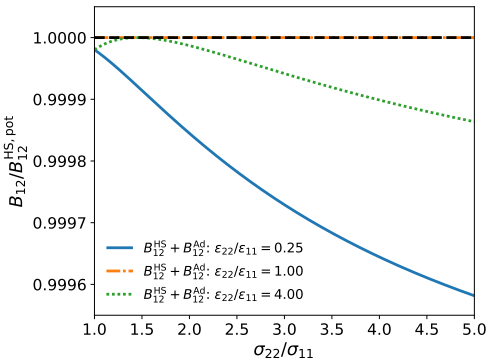

FIG. 2. The combined hard-sphere, B_{12}^{HS}, and extra term, B_{12}^{Ad}, contribution to the cross second virial coefficient plotted for the additive hard-sphere reference systems. $B_{12} = B_{12}^{\mathrm{HS}} + B_{12}^{\mathrm{Ad}}$ is plotted relative to the exact value, $B_{12}^{\mathrm{HS,pot}}$. The plot is made at $T^* = Tk_{\mathrm{B}}/\epsilon_{12} = 1.0$ for three different LJ-fluids at different $\epsilon_{22}/\epsilon_{11}$ ratios.

shows that the deviations are typically below 3% for a range of different combinations of $\epsilon_{22}/\epsilon_{11}$ and σ_{22}/σ_{11} ratios.

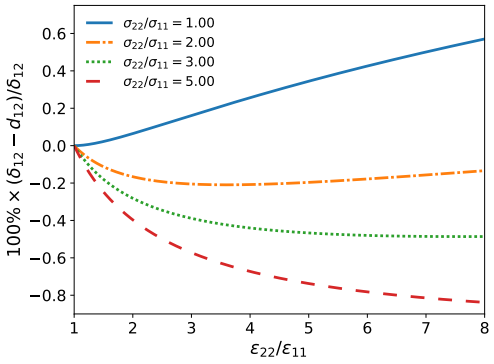

FIG. 3. The relative difference between the additive hard-sphere diameter, d_{ij}, and the Barker-Henderson hard-sphere diameter, δ_{ij}, plotted for different $\epsilon_{22}/\epsilon_{11}$-ratio. The plot is made using $T^* = Tk_{\mathrm{B}}/\epsilon_{12}$ for four different LJ-fluids at different σ_{22}/σ_{11} ratios.

B. A discussion of non-additivity

It is relevant to use a non-additive hard-sphere system as reference when the Barker–Henderson diameter of the cross interaction, δ_{ij} (Eq. (8)) is not additive, i.e. $\delta_{ij} \neq (\delta_{ii} + \delta_{jj})/2$. In the additive reference, this can be partly compensated for by including an

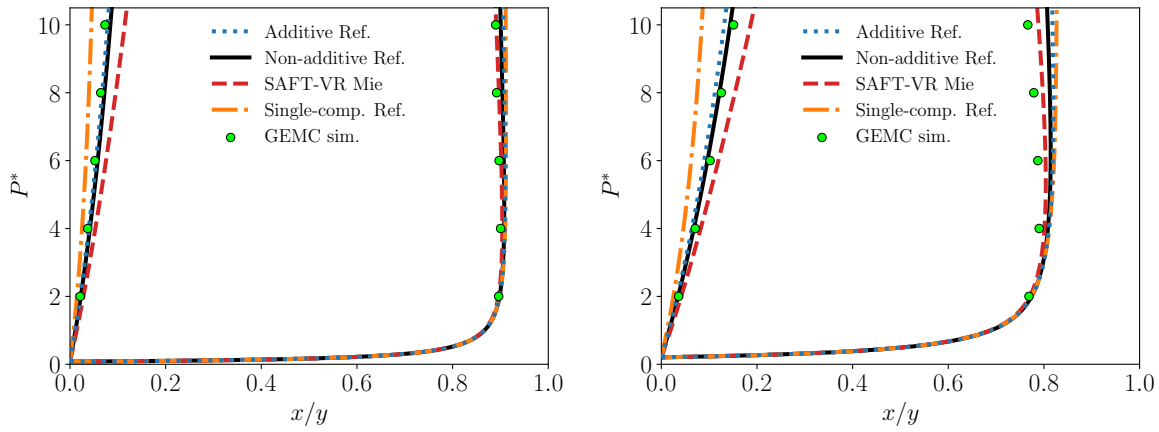

(a) $T^* = 7$. (b) $T^* = 8$.

FIG. 4. VLE of an LJ-mixture with $\sigma_{22}/\sigma_{11} = 1$, $\epsilon_{22}/\epsilon_{11} = 8$, and $k_{ij} = -0.1$. Two temperatures are shown: $T^* = 7$ (a) and $T^* = 8$ (b).

extra term in the perturbation theory (Eq. (16)). Leonard and co-workers argued that the extra term is usually small.[24] As a consequence, the term has been omitted from perturbation theories thus far.[2] To our knowledge, we present the first quantitative discussion of when the term becomes relevant.

A comparison of Fig. 1b (no extra term) with Fig. 2 (extra term included) shows that by including the extra term in the additive hard-sphere reference, the error in the cross virial coefficient of the hard-sphere mixture is reduced from 2% to below 0.02%. At most conditions however, we find that the extra term in the additive hard-sphere reference can safely be neglected because it is small, in accordance with the recommendations by Leonard et al.[24] A 2% error in the hard-sphere contribution to the cross second virial coefficient is arguably acceptable. Predictions from the perturbation theories with additive and non-additive references give mostly similar results. However, there are a few notable exceptions.

We find that accounting for non-additivity becomes important in systems where the $\epsilon_{22}/\epsilon_{11}$-ratio deviates significantly from unity, i.e. for mixtures where the well-depth of one fluid is much smaller than the other. This can be explained by Fig. 3, which shows that the relative difference between the additive hard-sphere diameter, d_{ij}, and the Barker-Henderson hard-sphere diameter, δ_{ij}, increases with higher $\epsilon_{22}/\epsilon_{11}$-ratios.

Figure 4 displays the VLE of a mixture of two LJ-fluids where $\sigma_{22}/\sigma_{11} = 1$, $\epsilon_{22}/\epsilon_{11} = 8$, and $k_{ij} = -0.1$. These ratios are relevant for the description of the helium–neon mixture

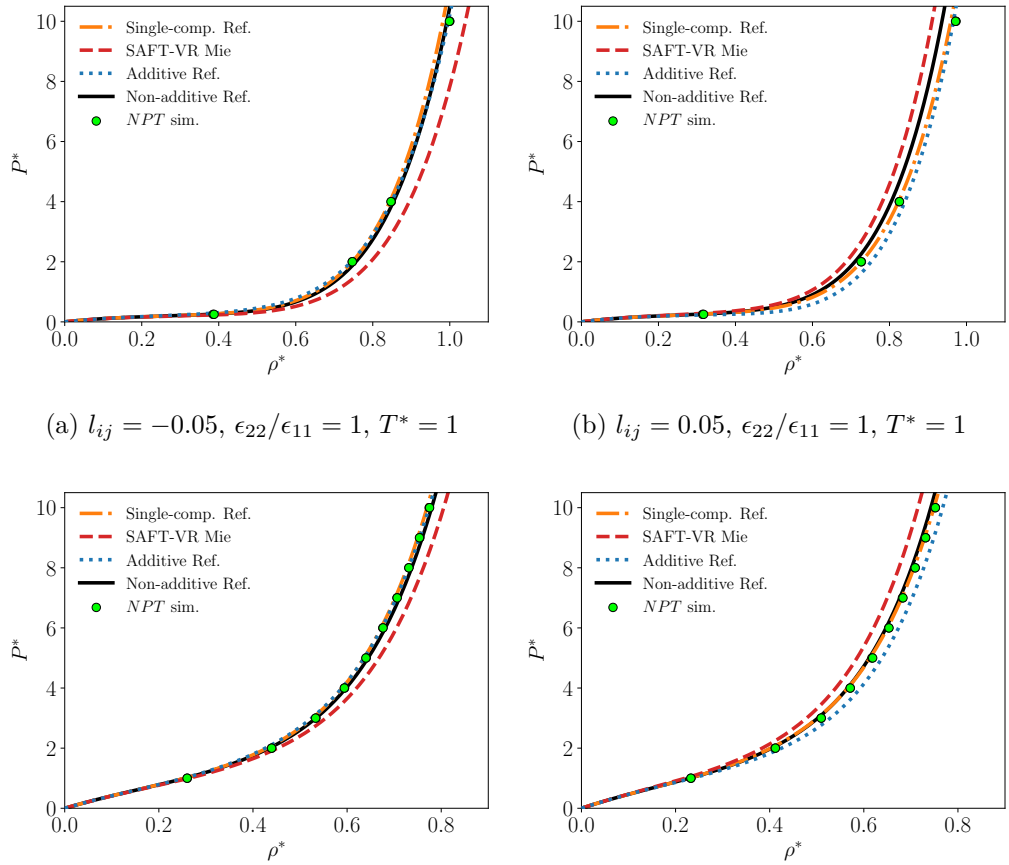

(a) $l_{ij} = -0.05$, $\epsilon_{22}/\epsilon_{11} = 1$, $T^* = 1$

(b) $l_{ij} = 0.05$, $\epsilon_{22}/\epsilon_{11} = 1$, $T^* = 1$

(c) $l_{ij} = -0.03$, $\epsilon_{22}/\epsilon_{11} = 4$, $T^* = 4.8$

(d) $l_{ij} = 0.05$, $\epsilon_{22}/\epsilon_{11} = 4$, $T^* = 4.8$

FIG. 5. The effect of deviations from the arithmetic combining rule for the σ parameter. For the mixtures in Figs. 4a–4d, $\sigma_{11} = \sigma_{22}$, $\sigma_{12} = (1 - l_{ij})\sigma_{11}$, and the composition is $x = 0.5$. The NPT simulation uncertainties are smaller than the symbol size.

with Feynman–Hibbs-corrected Mie potentials (see Ref. 46 for details). Fig. 4 displays visible deviations between GEMC simulation results and the predictions from the SAFT-VR Mie EoS (red dashed lines), in particular for the densest phase (to the left). This can be alleviated by 1) using a non-additive hard-sphere reference (full line), or by 2) including the extra term in Eq. (16) in the additive reference (dotted line). Fig. 4 also indicates that, for any choice of reference fluid, the agreement with simulations deteriorate as the critical pressure is approached at a fixed temperature, or the critical temperature is approached at a fixed pressure. This will be discussed further in Sec. IV C.

A second example where non-additivity becomes relevant is when $l_{ij} \neq 0$ in Eq. (5), i.e. when non-additivity is directly incorporated into the combining rule for σ_{ij}. A fitting

coefficient, $l_{ij} \neq 0$ is required in the modelling of the hydrogen–helium and the deuterium–helium mixtures with Feynman–Hibbs-corrected Mie potentials in order to reproduce the behavior of the cross second virial coefficient.[46] For real mixtures, deviations from additivity are expected to be small. Similar to the helium-hydrogen mixture discussed in Ref. 46, we shall consider $|l_{ij}| < 0.05$.

Fig. 5 shows the effect of the l_{ij} parameter on the pressure–density isotherms by using various reference systems. Since $\sigma_{11}/\sigma_{22} = 1$ for all of the examples shown in the figure, the single-component hard-sphere reference is expected to be reliable, at least based on the discussion in Sec. IV A. In fact, the single-component reference gives the most accurate representation of the pressure in all of the examples in Fig. 5. Nearly the same accuracy is obtained by using a non-additive hard-sphere reference. The red-dashed lines show that there are significant deviations between the NPT Monte Carlo simulations (the symbols) and SAFT-VR Mie, where non-additivity is not accounted for. Including the extra term as in the non-additive reference (solid-line) shifts the predictions in the right direction, albeit too much in some cases (see Figs. 5b and 5d). The overshoot from the additive hard-sphere reference is probably due to the representation of the radial distribution function at contact for the additive hard-sphere mixture (Eq. (19)), which is expected to deviate from simulation results.

For all of the cases displayed in Fig. 5, we observe that the agreement between the EoS predictions and the simulation results remains to a large extent unchanged if a_2 and a_3 are omitted from the computations. Hence, the plots in Fig. 5 primarily test the consistency and accuracy of a^{HS} and a_1, as well as the ability of the perturbation theory to approximate the actual Helmholtz energy of the reference fluid.

C. Poor representation of the critical region with increasing well-depth ratio

Fig. 6 compares the predictions from perturbation theories with different choices of reference with the simulation data from Vrabec et al.[47] and Potoff et al.[48] Here, $\sigma_{22}/\sigma_{11} = 1$, but different $\epsilon_{22}/\epsilon_{11}$ ratios have been considered. The figure displays no difference between the references, and all of them are in reasonable agreement with the simulation results.

Tab. III in Ref. 2 lists parameters of Mie-potentials that enable representation of real fluids. The table shows that fluids modelled by Mie fluids can have $\epsilon_{22}/\epsilon_{11}$-ratios that differ

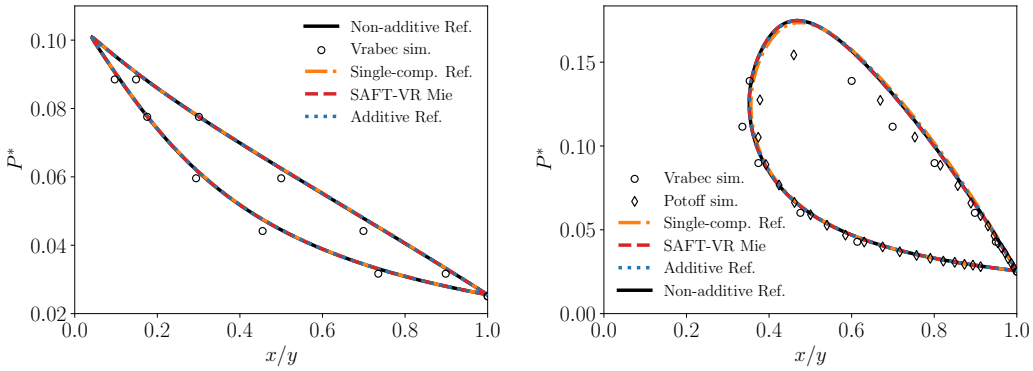

(a) $\epsilon_{22}/\epsilon_{11} = 0.75$ (b) $\epsilon_{22}/\epsilon_{11} = 0.5$

FIG. 6. A comparison of the predictions from the EoS with the data by Vrabec et al.[47] and Potoff et al.[48] For both cases, $\sigma_{11} = \sigma_{22} = 1$ and $T^* = 1$. Two ϵ-rations are plotted, $\epsilon_{22}/\epsilon_{11} = 0.75$ (a), and $\epsilon_{22}/\epsilon_{11} = 0.5$ (b).

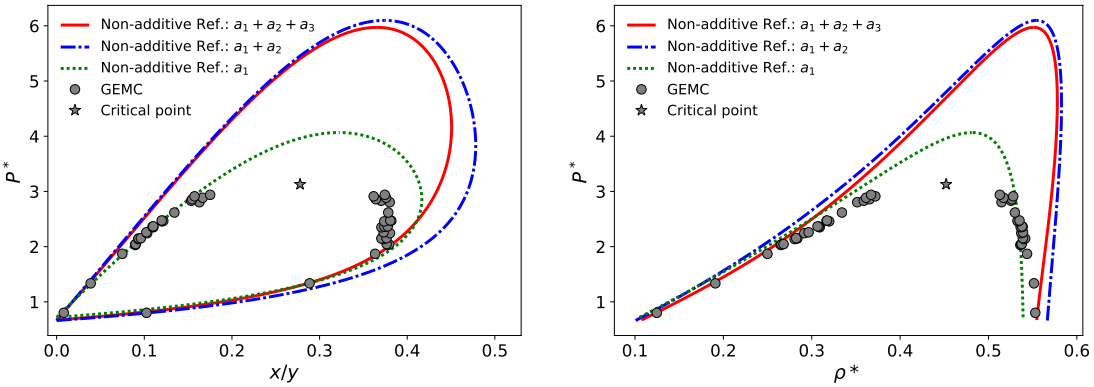

(a) P^*xy (b) $P^*\rho^*$

FIG. 7. An LJ-mixture with $\sigma_{22}/\sigma_{11} = 1$, $\epsilon_{22}/\epsilon_{11} = 8$, and $k_{ij} = -0.1$ at $T^* = 9.695$ with a non-additive reference and with varying order of perturbation terms included in the perturbation theory. P^*xy (a) and $P^*\rho^*$ (b) phase envelopes are plotted.

much more from unity than those showcased in Fig. 6. For instance, the toluene–fluorine mixture has a ratio exceeding four. Hence, it is relevant to have a perturbation theory that is able to represent mixtures with $\epsilon_{22}/\epsilon_{11}$-ratios deviating significantly from unity. All of the models seem to overpredict the pressures in vicinity of the critical point in Fig. 6b, where the $\epsilon_{22}/\epsilon_{11}$-ratio is only 0.5. This trend becomes more pronounced as the $\epsilon_{22}/\epsilon_{11}$-ratio differs even more from unity.

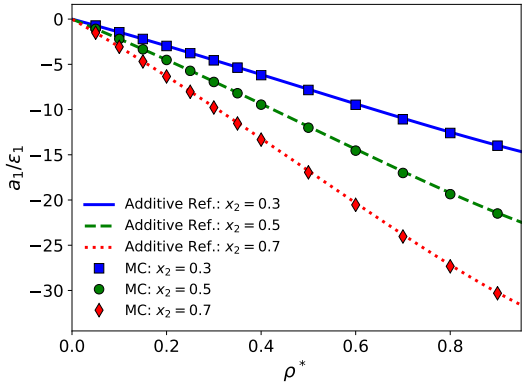

(a) First order perturbation term

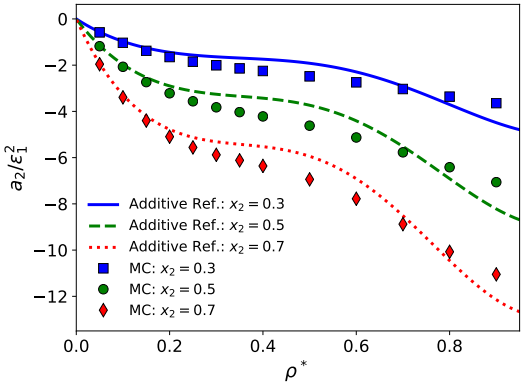

(b) Second order perturbation term

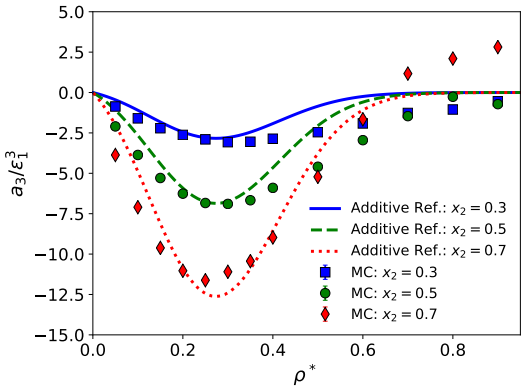

(c) Third order perturbation term

FIG. 8. Comparison of the perturbation theory with additive reference (lines) with canonical MC simulations for the reduced perturbation terms. An LJ mixture with $\sigma_{22} = \sigma_{11}$, $\epsilon_{22} = 8\epsilon_{11}$, and $k_{ij} = -0.1$ is simulated at $T^* = 9.695$. $N_2 \in \{150, 250, 350\}$, corresponding to mole fractions of Type 2 molecules of 30, 50, 70 %. One standard deviation of the sample mean is used for the error bars of the MC results of a_3 (c). The error bars are not included for a_1 (a) and a_2 (b) as the magnitude of the error is smaller than the symbol size.

Fig. 7 shows the phase envelopes of the same LJ-mixture as shown in Fig. 4, now at the higher temperature $T^* = 9.695$. In line with the trend established in Fig. 4, the deviations increase as the temperature is raised further toward the Type 2 molecule pure fluid critical temperature ($T^*_{\text{critical}} = 10.6$). In particular, the third order perturbation theory (solid line) overpredicts the critical pressure by nearly 100%. Gradually increasing the complexity of the perturbation theory by systematically incorporating higher order perturbation terms

reveals that when a_2 is included, the critical pressure shifts by a large amount away from the estimated critical pressure from GEMC simulations. This indicates that a_2 is poorly represented by the perturbation theory presented in Sec. II.

Further insight can be gained by investigating the perturbation terms, a_1–a_3 by use of NVT Monte Carlo simulations combined with the theory by Zwanzig[34] (See Sec. II A for details). To our knowledge, this is the first time this methodology has been used for mixtures, albeit results have been discussed for single-component fluids.[2,23] In the following, we shall examine the perturbation terms of the mixture displayed in Fig. 7 in further detail. Figure 8a shows that the first order perturbation term, a_1 is represented to a high accuracy. This indicates that the radial distribution function of the different components in the mixture resembles that in a pure fluid, which is expected as the particles of Type 1 and 2 are of equal size. Figs. 8b and 8c reveal large deviations between a_2 and a_3 from the perturbation theory and from Monte Carlo simulations. For example, the current correlation for a_3 always yields negative values, whereas the simulations show that it can be positive at high densities (Fig. 8c). We find that these deviations are present for all choices of reference, which all give similar overpredictions of the critical pressure in Figs. 6b and 7a (not shown). To further develop the representation of a_2 and a_3 for mixtures falls beyond the scope of this work, but is an important challenge for the future.

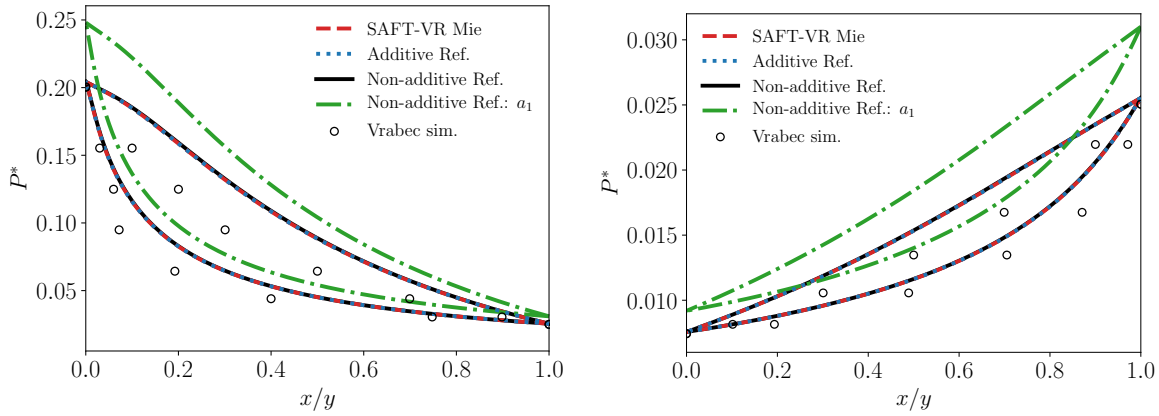

(a) $\sigma_{22}/\sigma_{11} = 0.5$ (b) $\sigma_{22}/\sigma_{11} = 1.5$

FIG. 9. Comparison of the different models with the experimental data by Vrabec et al.[47] For both fluids, $\epsilon_{11} = \epsilon_{22} = \epsilon_{12} = 1$, the σ_{11}/σ_{22} ratios are 0.5 (a) and 1.5 (b), and the temperature is $T^* = 1$. The single-component reference did not predict two phases in both cases.

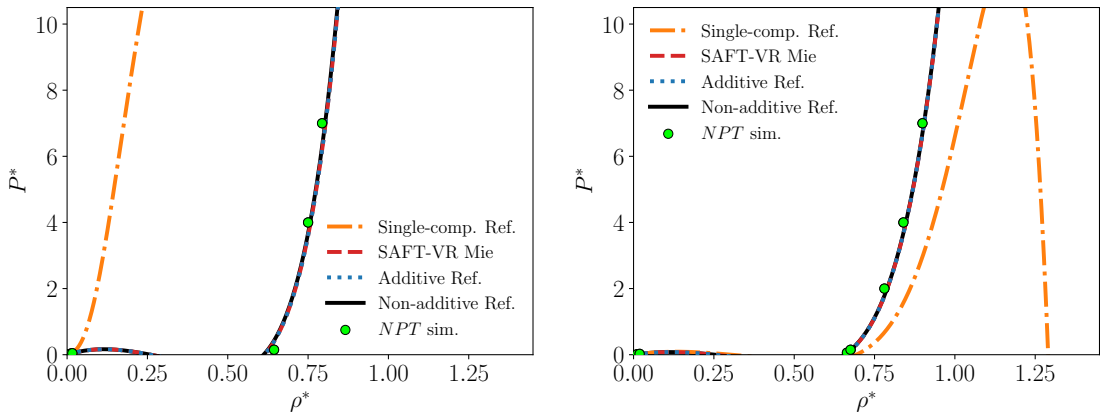

(a) $x_1 = 0.30$ (b) $x_1 = 0.70$

FIG. 10. Pressure–density isotherms for an additive mixture with $\sigma_{22}/\sigma_{11} = 0.5$ and $\epsilon_{11} = \epsilon_{22} = \epsilon_{12}$ at $T^\star = 1$. For this mixture, SAFT-VR Mie, the additive reference, and the non-additive reference are equivalent. Two different molar fractions are plotted, $x_1 = 0.30$ (a), and $x_1 = 0.70$ (b).

D. Inaccurate representation of mixtures with different particle sizes

For mixtures where $\sigma_{22}/\sigma_{11} = 1$, the single-component hard-sphere reference has given similar results for the phase envelopes as the other references. Fig. 9 displays phase envelopes of mixtures with size-asymmetric molecules. Only results with the additive and non-additive hard-sphere references are shown, since the single-component reference failed to predict two phases. Fig. 10 shows that the pressure-density isotherms from the single-component reference deviate by a large amount from the results from the NPT Monte Carlo simulations, while the simulations display agreement with the other two references (solid lines). This explains why the single-component reference does not give two phases.

The failure of the single-component reference for high σ_{22}/σ_{11}-ratios was already seen for the cross-virial coefficient discussed in Sec. IV A. However, arguably the most important cause of its mispredictions can be attributed to the representation of a_1. The variable x_0 is defined for the different references in Eq. (43). For a single-component LJ fluid, the typical interval of x_0 is $1.02 < x_0 < 1.11$, where the highest ratio is encountered at $T^* = 10$. The same interval is encountered when evaluating $x_{0,ij}$ in additive and non-additive hard-sphere mixtures. For the single-component hard-sphere reference, on the other hand, $x_{0,ij}$ can be both above and below 1. For the mixture displayed in Fig. 9b, we find that $0.7 < x_{0,ij} < 1.55$ for the single-component reference. In principle, $a_{1,ij}$ as defined by the integral in Eq. (36) can be

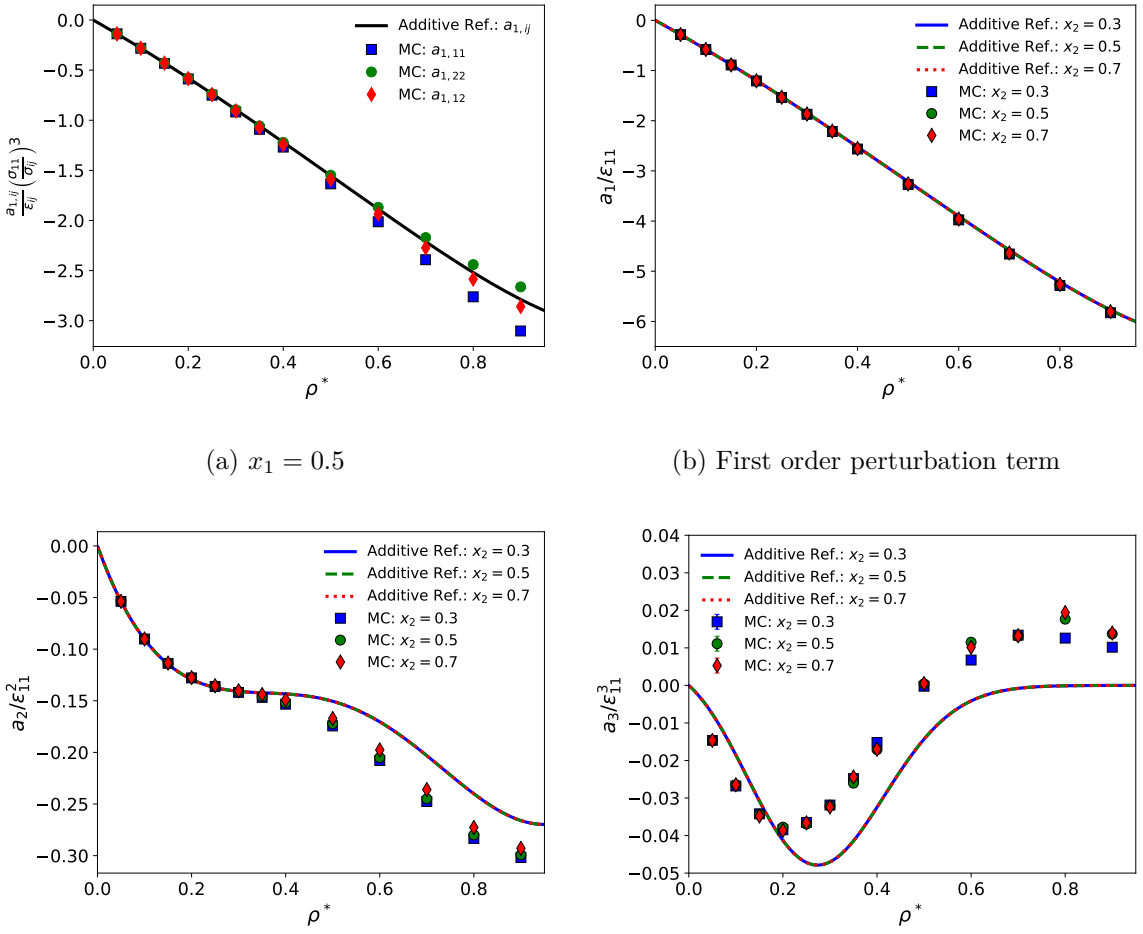

(a) $x_1 = 0.5$

(b) First order perturbation term

(c) Second order perturbation term

(d) Third order perturbation term

FIG. 11. Comparison of perturbation theory with an additive reference (lines) with canonical MC simulations for the reduced perturbation terms. An LJ mixture with $\sigma_{22}/\sigma_{11} = 1.5$, $\epsilon_{11} = \epsilon_{22}$ is simulated at $T^* = 1$. $N_2 \in \{150, 250, 350\}$, corresponding to mole fractions of Type 2 molecules of 30, 50, 70 %. In a) the configurational energy contribution from the 11, 22 and 12 pair interactions are plotted for a composition of $x_1 = 0.5$. b)-d) Mixture perturbation terms. One standard deviation of the sample mean is used for the error bars of the canonical MC results of a_3 (d). The error bars are not included for a_1 (b) and a_2 (c) as the magnitude of the error is smaller than the symbol size.

evaluated by numerical integration. This is usually not done in practical implementations of perturbation theories, as it gives unfeasible computational times. Instead, the correlations presented in Sec. II B 1 are used. By comparing to a numerical integration of Eq. (36) (not shown), we find that these correlations are grossly inaccurate in the interval where

the single-component reference operates in mixtures where σ_{22}/σ_{11} deviate from one. To use the single-component reference for such mixtures, these correlations must be improved. However, as the inherent accuracy of this reference is limited, as discussed in Sec. II B 1, there are few arguments to proceed along this route.

Fig. 9 shows that the predictions from the perturbation theories with the additive and non-additive references lie above the simulations results by Vrabec et al.[47] To verify whether these simulations were accurate, we performed independent GEMC simulations that were found to be in excellent agreement with previous simulation results (not shown).

For particles with σ_{22}/σ_{11}-ratios that differ from one, the radial distribution function of the mixture can differ significantly from that of the pure fluid, in particular at high densities. It is then questionable whether using the pure component radial distribution function in the expression for a_1 (Eq. (36)) is a good assumption. We tested this assumption by obtaining the independent terms from the different interactions, $a_{1,ij}$, by use of MC simulations (see Sec. III A) and used this to compute a_1 of the mixture numerically with Eq. (36). The resulting values for $a_{1,ij}$ (symbols) differ from the approximation facilitated by Eq. (39), which gives only one solid-line for all of the $i-j$ pairs, as shown in Fig. 11a. However, when weighted with the mole-fractions, Fig. 11b demonstrates that the a_1-value from the perturbation theory (lines) is in excellent agreement with the a_1 obtained with MC simulations (symbols, See Sec. III A for details). This suggests that replacing the pair correlation function of the mixture with that of the pure component at the same effective hard-sphere diameter gives a reasonable representation of a_1, even though the $a_{1,ij}$-values differ. However, we cannot rule out the possibility that small deviations in a_1 are responsible for some of the deviations in Fig. 9.

Figs. 11c and 11d reveal large deviations between a_2 and a_3 from the perturbation theory, and the corresponding values from the MC simulations, in particular at high densities. At $T^* = 1$ and for a fixed density, both a_2 and a_3 are uniquely defined in the perturbation theory described in Sec. II, since the α-value of the mixture is fixed. This explains why the solid lines for all the compositions overlap in Figs. 11c and 11d. The simulation results however, do not reproduce this behavior, and there is a clear distinction between a_2 and a_3 values obtained at different compositions. This shows that the expressions for a_2 and a_3 fail to reproduce the qualitative behavior of the perturbation terms, even for moderate differences in the particles sizes. The overprediction of the phase equilibrium pressures in

Fig. 9 is largely due to the mispredictions of a_2 at higher densities (cf. Fig. 11c): we tested that setting a_3 to zero in the perturbation theories did not alter the phase envelopes, whereas also setting a_2 to zero changed it significantly (green curve in Fig. 9).

V. CONCLUSION

This work addresses the fundamentals of perturbation theory for mixtures. The starting point was the SAFT-VR Mie equation of state, which is a perturbation theory for Mie fluids that uses a third-order Barker–Henderson expansion of the Helmholtz energy. Three different hard-sphere reference systems were compared: 1) single-component, 2) additive mixture and 3) non-additive mixture. Binary mixtures of Lennard-Jones (LJ) fluids were investigated to evaluate the accuracy of the different formulations, where the ratios of the well-depths (ϵ) and position where the interaction potential equals zero (σ) were varied.

Only the non-additive hard-sphere reference reproduced the exact result for the hard-sphere contribution to the cross-virial coefficient. The additive hard-sphere reference deviated less than 3% from the exact results. The situation could be improved by incorporating an extra term in the perturbation theory that is usually neglected, which reduced the error to 0.02%. The pure-component reference gave poor predictions when the σ-ratio of the binary mixture deviated from unity.

Accounting for non-additivity was found to be important to accurately predict the solubility of mixtures with high ϵ-ratios and when non-additivity was explicitly incorporated into the mixing rule for σ. In these cases, the non-additive hard-sphere reference is preferred, but the single-component reference was most accurate when the σ-ratio was one.

For all cases investigated except for the single-component reference, comparison to Monte Carlo simulations in the canonical ensemble showed that the first order perturbation term, a_1, was represented to a high accuracy. To approximate the radial distribution function of the mixture by that of the pure-component fluid at the corresponding hard-sphere diameter was found to be a good assumption for a_1. We found significant deviations between theory and simulations for the second and third order perturbation terms, a_2 and a_3, for mixtures with ϵ- and σ-ratios that deviated from unity. In these mixtures, the perturbation theory failed to predict the phase equilibrium envelopes regardless of reference, in particular close to critical states.

Further development of the perturbation theory for such mixtures is an important task for the future, as mixtures described by Mie-fluids with ϵ- and σ-ratios similar to those addressed in the present work are important in many natural and industrial applications.

ACKNOWLEDGMENTS

The authors thank Erich A. Müller, Amparo Galindo and George Jackson for helpful discussions. Ailo Aasen and Øivind Wilhelmsen have been supported by the ENERSENSE initiative for which they are grateful. Morten Hammer, Ailo Aasen, Åsmund Ervik and Øivind Wilhelmsen have been supported by the HYVA project, which is part of the Strategic Institute Programme of SINTEF Energy Research funded through the Basic Research Funding scheme of the Research Council of Norway.

REFERENCES

[1]J. Gross and G. Sadowski, Ind. Eng. Chem. Res. **40**, 1244 (2001).

[2]T. Lafitte, A. Apostolakou, C. Avendaño, A. Galindo, C. S. Adjiman, E. A. Müller, and G. Jackson, J. Chem. Phys. **139**, 154504 (2013).

[3]A. Dominik, W. G. Chapman, M. Kleiner, and G. Sadowski, Ind. Eng. Chem. Res. **44**, 6928 (2005).

[4]J. Rozmus, J.-C. de Hemptinne, A. Galindo, and P. Mougin, Ind. Eng. Chem. Res. **52**, 9979 (2013).

[5]P. Paricaud, A. Galindo, and G. Jackson, Fluid Phase Equilib. **194-197**, 87 (2002), proceedings of the Ninth International Conference on Properties and Phase Equilibria for Product and Process Design.

[6]E. Razavi, A. Khoshsima, and R. Shahriari, Ind. Eng. Chem. Res. **58**, 11038 (2019).

[7]A. Gil-Villegas, A. Galindo, P. J. Whiteheat, S. J. Mills, and G. Jackson, J. Comput. Phys. **106**, 4168 (1997).

[8]J. Li, H. He, C. Peng, H. Liu, and Y. Hu, Fluid Phase Equilib. **276**, 57 (2009).

[9]L. A. Davies, A. Gil-Villegas, and G. Jackson, Int. J. Thermophys. **19**, 675 (1998).

[10]I. Nezbeda, R. Melnyk, and A. Trokhymchuk, Fluid Phase Equilib. **309**, 174 (2011).

[11]K. E. Gubbins, Mol. Phys. **111**, 3666 (2013).

[12]K. E. Gubbins, Fluid Phase Equilib. **416**, 3 (2016).

[13]S. H. Huang and M. Radosz, Ind. Eng. Chem. Res. **29**, 2284 (1990).

[14]T. Kraska and K. E. Gubbins, Ind. Eng. Chem. Res. **35**, 4727 (1996).

[15]F. J. Blas and L. F. Vega, Ind. Eng. Chem. Res. **37**, 660 (1998).

[16]S. Tamouza, J.-P. Passarello, P. Tobaly, and J.-C. de Hemptinne, Fluid Phase Equilib. **222-223**, 67 (2004).

[17]Y. Peng, K. D. Goff, M. C. dos Ramos, and C. McCabe, Fluid Phase Equilib. **277**, 131 (2009).

[18]A. Lymperiadis, C. S. Adjiman, A. Galindo, and G. Jackson, J. Chem. Phys. **127**, 234903 (2007).

[19]Ø. Wilhelmsen, A. Aasen, G. Skaugen, P. Aursand, A. Austegard, E. Aursand, M. A. Gjennestad, H. Lund, G. Linga, and M. Hammer, Ind. Eng. Chem. Res. **56**, 3503 (2017).

[20]E. Moine, A. Piña-Martinez, J.-N. Jaubert, B. Sirjean, and R. Privat, Ind. Eng. Chem. Res. **58**, 20815 (2019).

[21]J. A. Barker and D. Henderson, J. Chem. Phys. **47**, 4714 (1967).

[22]D. A. McQuarrie, *Statistical Mechanics* (Harper & Row, New York, 1976).

[23]T. van Westen and J. Gross, J. Chem. Phys. **147**, 014503 (2017).

[24]P. J. Leonard, D. Henderson, and J. A. Barker, Trans. Faraday Soc. **66**, 2439 (1970).

[25]H. C. Andersen, J. D. Weeks, and D. Chandler, Phys. Rev. A **4**, 1597 (1971).

[26]J. D. Weeks, D. Chandler, and H. C. Andersen, J. Chem. Phys. **54**, 5237 (1971).

[27]L. Lee and D. Levesque, Mol. Phys. **26**, 1351 (1973).

[28]A. Santos, M. Loópes de Haro, and S. B. Yustec, J. Chem. Phys. **122**, 024514 (2005).

[29]R. Fantoni and A. Santos, Phys. Rev. E **84**, 041201 (2011).

[30]A. H. Harvey and J. M. Prausnitz, Fluid Phase Equilib. **48**, 197 (1989).

[31]T.-K.-H. Trinh, J.-P. Passarello, J.-C. de Hemptinne, and R. Lugo, Fluid Phase Equilib. **429**, 177 (2016).

[32]P. Sillrén and J.-P. Hansen, Mol. Phys. **105**, 1803 (2007).

[33]T. Boublík, J. Chem. Phys. **53**, 471 (1970).

[34]R. W. Zwanzig, J. Chem. Phys. **22**, 1420 (1954).

[35]N. F. Carnahan and K. E. Starling, J. Chem. Phys. **51**, 635 (1969).

[36]G. A. Mansoori, N. F. Carnahan, K. E. Starling, and T. W. Leland Jr., J. Chem. Phys. **54**, 1523 (1971).

[37]A. Mulero, *Theory and Simulation of Hard-Sphere Fluids and Related Systems* (Springer, Berlin, 2008).

[38]P. Paricaud, Phys. Rev. E **78**, 021202 (2008).

[39]A. Aasen, M. Hammer, Å. Ervik, E. A. Müller, and Ø. Wilhelmsen, J. Chem. Phys. **151**, 064508 (2019).

[40]J. M. Prausnitz, R. N. Lichtenthaler, and E. G. de Azevedo, *Molecular Thermodynamics of Fluid-Phase Equilibria*, third edition ed. (Prentice Hall, 1999).

[41]A. Aasen, M. Hammer, G. Skaugen, J. Jakobsen, and Ø. Wilhelmsen, Fluid Phase Equilib. **442**, 125 (2017).

[42]M. L. Michelsen and J. M. Mollerup, *Thermodynamic models: Fundamentals & computational aspects*, 2nd ed. (Tie-Line Publications, Holte, Denmark, 2007).

[43]A. Panagiotopoulos, N. Quirke, M. Stapleton, and D. Tildesley, Mol. Phys. **63**, 527 (1988).

[44]M. Allen and D. Tildesley, *Computer Simulation of Liquids*, 2nd ed. (Oxford University Press, New York, 2017).

[45]D. Frenkel and B. Smit, *Understanding Molecular Simulation: From Algorithms to Applications*, 2nd ed. (Academic Press, New York, 2002).

[46]A. Aasen, M. Hammer, E. A. Müller, and Ø. Wilhelmsen, J. Chem. Phys. (2019).

[47]J. Vrabec, A. Lotfi, and J. Fischer, Fluid Phase Equilib. **112**, 173 (1995).

[48]J. J. Potoff and A. Z. Panagiotopoulos, J. Comput. Phys. **109**, 10914 (1998).